

# Bipolar luminescent materials containing pyrimidine terminals: synthesis, photophysical properties and a theoretical study†

Cite this: *RSC Adv.*, 2013, **3**, 21877

Jiena Weng,<sup>a</sup> Qunbo Mei,<sup>\*a</sup> Quli Fan,<sup>a</sup> Qidan Ling,<sup>a</sup> Bihai Tong<sup>c</sup> and Wei Huang<sup>\*ab</sup>

A new series of 4-monosubstituted pyrimidine bipolar materials containing a carbazole (**PM1–PM2**) or a triphenylamine (**PM3–PM5**) moiety as the electron donor have been synthesized by a ZnCl<sub>2</sub>-catalyzed three-component coupling reaction. These 4-monosubstituted pyrimidine compounds were characterized by UV-vis and fluorescence spectroscopy, cyclic voltammetry, as well as density functional theory (DFT) calculations. It was intriguing to find that these 4-monosubstituted pyrimidine compounds exhibited bright fluorescence with excellent quantum yields (~0.53–0.93) in the blue region. **PM1** and **PM2** had a lower LUMO than that of CBP (4,4'-di(9*H*-carbazol-9-yl)biphenyl), meaning that both of them had better electron injection and transfer abilities. The variation tendencies of energy levels and absorption spectra obtained from DFT calculations agreed well with those from experiment. Other electronic properties including ionization potentials (IP), electronic affinities (EA), and reorganization energies ( $\lambda_{\text{hole}}$  and  $\lambda_{\text{electron}}$ ) have been theoretically studied as well. These electronic properties could be tuned by introducing a different number of pyrimidin-4-yl moieties onto the donor fragments. The incorporation of pyrimidin-4-yl can significantly decrease the  $\lambda_{\text{electron}}$  and then improve the electron-accepting and hole–electron charge balance abilities. The combined theoretical and experimental studies offer insights into the nature of bipolar molecules containing 4-monosubstituted pyrimidine moieties, and provided a fertile ground for the design of appropriate ambipolar materials for optoelectronic applications.

Received 15th July 2013  
Accepted 20th August 2013

DOI: 10.1039/c3ra43631d

[www.rsc.org/advances](http://www.rsc.org/advances)

## Introduction

Since the first report of organic light-emitting diodes (OLEDs),<sup>1</sup> many studies have focused on designing and synthesizing highly efficient materials in order to improve the device efficiency.<sup>2–7</sup> One of the critical requirements for organic light emitting material is its carrier transport property. A large number of emitters and host materials have been developed with building blocks of carbazole<sup>2,6–15</sup> or triphenylamine (TPA),<sup>2,3,15,16</sup> well-known electron donors. Many of these materials favor injection/diffusion of holes over electrons and result in unbalanced charge injection into an emitting material layer (EML), and present essentially a so-called unipolar

character.<sup>16–19</sup> In order to circumvent this issue, considerable efforts have been placed into the development of bipolar materials with building blocks of both electron donors and acceptors.<sup>2,6,20–24</sup> Some common electron acceptors, including benzimidazole,<sup>25–28</sup> 1,3,4-oxadiazole,<sup>22,29,30</sup> triazine,<sup>31–33</sup> pyridine,<sup>14,34</sup> pyrimidine,<sup>14</sup> phosphine oxide,<sup>35–39</sup> and so on, were introduced into  $\pi$ -conjugated systems to develop novel materials with improved electron mobility.

Among these blocks of electron acceptors, the pyrimidine unit has only very rarely been incorporated into blocks of electron donors to develop ambipolar materials, although the pyrimidine group had a higher electron affinity than pyridine.<sup>40</sup> The introduction of the pyrimidine moiety was expected to improve the electron affinity of the material,<sup>41</sup> which made the pyrimidine moiety an attractive electron acceptor candidate to construct ambipolar materials. For example, blue OLEDs employing 2,7-bis[2-(4-*tert*-butylphenyl)pyrimidine-5-yl]-9,9'-spirobifluorene (TBPSF) as an emitter or the emitting host exhibited high currents over 5000 mA cm<sup>-2</sup>.<sup>42</sup> High efficiencies were achieved for red phosphorescent OLEDs based on 4,6-bis[3-(carbazol-9-yl)phenyl]pyrimidine, which is an ambipolar host material with a pyrimidine core.<sup>14</sup> The pyrimidine core improved the electron injection and carrier balance and thus reduced triplet exciton–polaron quenching at high current

<sup>a</sup>Key Laboratory for Organic Electronics & Information Displays, Institute of Advanced Materials, Nanjing University of Posts & Telecommunications, Nanjing 210046, China. E-mail: iamqbmei@njupt.edu.cn; iamwhuang@njupt.edu.cn; Fax: +86 25 8586 6533; Tel: +86 25 8586 6396

<sup>b</sup>Jiangsu-Singapore Joint Research Center for Organic/Bio-Electronics & Information Displays, Institute of Advanced Materials, Nanjing University of Technology, Nanjing 211816, China. Fax: +86 25 5813 9988; Tel: +86 25 5813 9001

<sup>c</sup>Institute of Molecular Engineering and Applied Chemistry, College of Metallurgy and Resources, Anhui University of Technology, Ma'anshan, Anhui 243002, P. R. China

† Electronic supplementary information (ESI) available: <sup>1</sup>H NMR, <sup>13</sup>C NMR, MS spectra and additional data. See DOI: 10.1039/c3ra43631d

density. Most recently, extremely low turn-on voltages for fac-tris(2-phenylpyridine)iridium(III) (Ir(PPy)<sub>3</sub>)-based green phosphorescent OLEDs were achieved by utilizing pyrimidine-containing electron transport materials as an electron-transport and hole/excition-block lay.<sup>43</sup>

The pyrimidine ring was attractive to us for its high electron affinity.<sup>40,44</sup> As far as we know, although efficient pyrimidine-containing host materials<sup>14,45</sup> and electron transport materials<sup>43,46</sup> have been reported, almost all of these materials were constructed with a pyrimidine core and there was no report on the electronic properties of luminescent materials containing a 4-monosubstituted pyrimidine moiety. Herein, a series of bipolar molecules (**PM1–PM5**, Scheme 1), containing the electron acceptor of pyrimidine and the electron donor of carbazole or triphenylamine, were designed. Our current work focuses on the relationships of molecular structure and photoelectric property of the **PM** (including **PM1–PM5**) compounds. The photophysical and electronic properties of the **PM** compounds were systematically varied by chemical modification. In addition, density functional theory (DFT) and time-dependent density functional theory (TD-DFT) calculations were also presented to predict the photoelectric properties of the **PM** compounds.

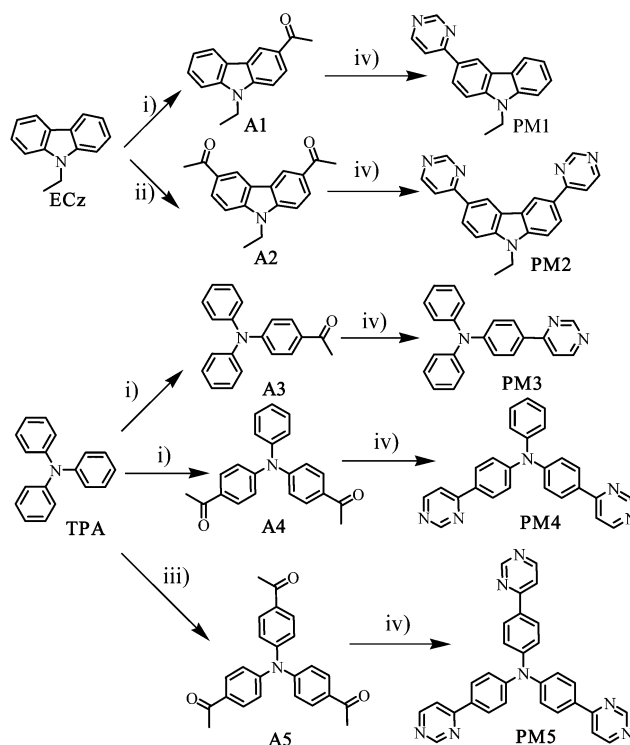
## Results and discussion

### Synthesis

Many methods, including the Leuckart reaction<sup>47</sup> and the Brederick-type<sup>48,49</sup> synthesis method, were available for the synthesis of 4-arylpyrimidine compounds from aromatic ketones. For example, Helland and Lejon<sup>50</sup> reported the synthesis of 4-phenylpyrimidine from condensation of acetophenone with formamide at 179 °C for 17 h in the presence of cuprous chloride as an oxidant. Another simple and single step synthesis of 4-arylpyrimidine using a combination of ketones, formamide and a source of ammonia under microwave irradiation was also reported later.<sup>49</sup> We had try to synthesise our target products **PM1–PM5** (Scheme 1) from the corresponding ketones (**A1–A5**) using the two methods mentioned above. Unfortunately, the formation of the corresponding formyl amide, a major side product, resulted in a decrease in the product yield and difficult purification. As shown in Scheme 1, the third method we had adopted was a ZnCl<sub>2</sub>-catalyzed three-component coupling reaction involving aromatic ketones, triethyl orthoformate, and ammonium acetate, which led to the production of 4-substituted pyrimidine derivatives in a single step.<sup>51</sup> Although the product yields (14.5% to 20%) were still unsatisfying, the target **PM** products could be purified simply by silica gel chromatography. The structures of the target products were identified by using <sup>1</sup>H NMR, <sup>13</sup>C NMR, and GC-MS or MALDI-TOF-MS.

### Photophysical properties

The UV-vis absorption spectra of the **PM** compounds investigated in this work were recorded in diluted solution and in the solid state (see Table 1 and Fig. 1). As shown in Fig. 1, the origin



**Scheme 1** Synthetic routes of **PM1–PM5**. Conditions: (i) AlCl<sub>3</sub>, acetic anhydride, DCM, 0 °C to room temperature (RT); (ii) AlCl<sub>3</sub>, acetyl chloride, DCM, 0 °C to RT; (iii) AlCl<sub>3</sub>, acetyl chloride, DCM, 0–40 °C; (iv) triethyl orthoformate, ammonium acetate, ZnCl<sub>2</sub>, toluene, 100 °C.

of the lowest energy band in the absorption spectra of **PM1–PM5** was due to an intramolecular  $\pi \rightarrow \pi^*$  charge transfer (ICT)<sup>52,53</sup> from the donor (carbazole or TPA)-based molecular orbitals to the acceptor (pyrimidine)-based molecular orbitals in the relevant dipolar compounds. The absorption band at around 300 nm of **PM1–PM3** could be assigned to the carbazole/TPA-centered  $n \rightarrow \pi^*$  transition. For **PM1–PM2**, compared to the carbazole-centered  $n \rightarrow \pi^*$  transition band, the absorbance at the lowest energy band increased with the introduction of more pyrimidin-4-yl moieties. Meanwhile, it was obviously observed from Fig. 1(c) and (d) that the TPA-centered  $n \rightarrow \pi^*$

**Table 1** Optical properties of **PM1–PM5**

Molecule	Solution <sup>a</sup>			Solid film <sup>b</sup>	
	$\lambda_{\text{abs}}$ (nm)	$\lambda_{\text{PL}}$ (nm)	$\Phi_{\text{F}}$	$\lambda_{\text{abs}}$ (nm)	$\lambda_{\text{PL}}$ (nm)
<b>PM1</b>	248, 300, 337	412	0.92	232, 302, 341	424.6
<b>PM2</b>	271, 308, 353	397	0.93	270, 305, 356	423.8
<b>PM3</b>	251, 300, 370	487	0.70	257, 302, 374	472
<b>PM4</b>	253, 351, 389	472	0.65	255, 353, 389	471
<b>PM5</b>	255, 384	464	0.53	258, 384	473.8

<sup>a</sup> The values of absorption and photoluminescence spectra were recorded in DCM. Excitation wavelength = 360 nm for measurements of photoluminescence spectra and  $\Phi_{\text{F}}$ . The  $\Phi_{\text{F}}$  values recorded are relative to that of 9,10-diphenylanthracene (0.90 in cyclohexane).

<sup>b</sup> Excitation wavelength = 360 nm for measurements of photoluminescence spectra.

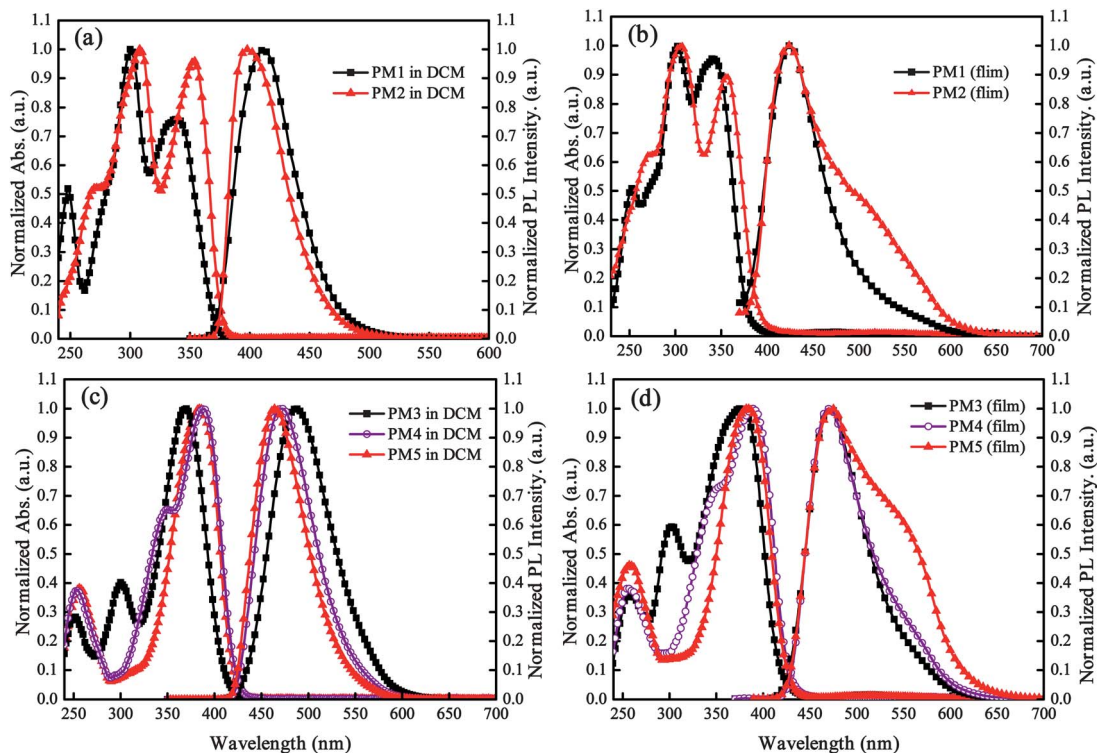


Fig. 1 Absorption and photoluminescence spectra ( $\lambda_{\text{ex}} = 360$  nm) of **PM1–PM5** in the DCM solution state (a), (c) and the thin film state (b), (d).

transition band red-shifted from **PM3** to **PM4**, and finally disappeared for **PM5**. This could be attributed to stronger ICT formed between the central donor and the outer pyrimidine. Absorption maxima were found to undergo a bathochromic shift by *ca.* 12 nm and 19 nm for **PM2** and **PM4** as compared to **PM1** and **PM3**, respectively, owing to an increased conjugation in **PM2** and **PM4**. However, with the number of pyrimidin-4-yl moiety increasing in the TPA-based compound, the lowest energy band maxima of **PM5** was slightly blue-shifted relative to **PM4**. It was probably due to the symmetrical geometry and relatively small dipole moment of **PM5** when compared to **PM4**, which is demonstrated by DFT calculations below. UV-vis absorption spectra of spin coating films for the **PM** compounds on quartz substrates measured at room temperature are shown in Fig. 1(b) and (d), which were almost similar to those in dilute dichloromethane (DCM) solution. The nearly identical absorption spectra in solution and in film suggested that there was minimal intermolecular interaction in the ground state in the thin film.

Upon excitation at 360 nm, **PM1–PM5** exhibited intense fluorescence in DCM at room temperature. The fluorescence quantum yields of **PM1–PM5** in DCM solution were measured to be  $\sim 0.53$ – $0.93$  relative to 9,10-diphenylanthracene (Table 1). A blue-shift of the emission spectra was observed with introduction of more pyrimidin-4-yl moieties, which was not affected by the increased conjugation. The thin film emission spectra were considerably different from those recorded in dilute DCM solution. The thin film emissions of **PM1** and **PM2** were red-shifted by *ca.* 13 nm and 27 nm relative to the corresponding

emissions in DCM, respectively. In addition, broad emissions ranging from 330 nm to 650 nm were observed from the thin films of **PM1** and **PM2**, which were considerably broader than those observed in solution. Compared with the thin film emission spectra of **PM1** and **PM2**, a distinct emission shoulder peak at around 500 nm came out with the introduction of two pyrimidin-4-yl moieties. This could be affirmed by comparing the thin film emission spectra of the TPA-based compounds, **PM3–PM5**. The long wavelength emission peaks could be possibly attributed to the intermolecular interactions in the excited state occurring in the solid state or by the formation of excimers.

For each **PM** molecule, weak solvatochromism was observed in the ICT absorption band. As shown in Fig. 2(a), the ICT absorption maximum of **PM5** red-shifted from 322 nm in nonpolar *n*-hexane to 343 nm in highly polar methanol. Similar data for the other **PM** compounds are shown in the supporting information (Fig. S1<sup>†</sup>). The optical absorption properties of five **PM** molecules in solvents of varying polarity are summarized in Table S1.<sup>†</sup> While the effect of solvent polarity on the absorption spectra was minimal, the fluorescence spectra of each **PM** molecule in polar solutions were significantly broadened and red-shifted when compared with those obtained in *n*-hexane (Fig. 2(b) and S2<sup>†</sup>). Thus, the solvatochromic effect was related to a decrease in the energy of the singlet excited state because of the reorientation or relaxation of the solvent dipoles.<sup>54</sup>

To study in more detail the solvatochromism, a Lippert–Magada plot (Fig. 3) was constructed, which described the

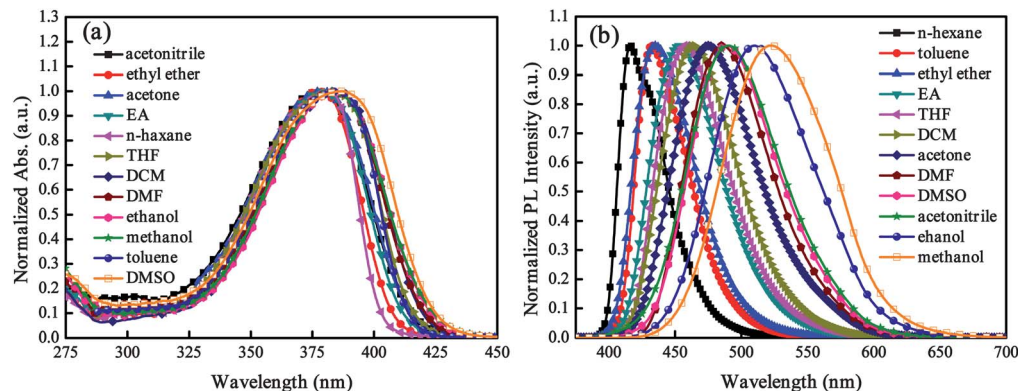


Fig. 2 Normalized absorption (a) and photoluminescence ((b),  $\lambda_{\text{ex}} = 360$  nm) spectra of **PM5** recorded in different solvents.

dependence of Stokes shifts (expressed in wavenumbers) on the orientation polarizability  $\Delta f$  derived from eqn (1).

$$\Delta f = \frac{(\varepsilon - 1)}{(2\varepsilon + 1)} - \frac{(n^2 - 1)}{(2n^2 + 1)} \quad (1)$$

According to the Lippert equation,<sup>54</sup> Stokes shift is proportional to the square of the change in dipole moments between the ground and excited states:

$$\nu_{\text{abs}} - \nu_{\text{em}} = \frac{2(\mu_{\text{e}} - \mu_{\text{g}})^2}{\hbar c a^3} \Delta f + C$$

where  $\varepsilon$  is the solvent dielectric constant and  $n$  is the solvent refractive index,  $\hbar$  is the Planck constant,  $c$  is the speed of light,  $\nu_{\text{abs}}$  and  $\nu_{\text{em}}$  are the wavenumbers of absorption and emission, respectively ( $\text{cm}^{-1}$ ),  $a$  is the Onsager radius,  $\mu_{\text{e}} - \mu_{\text{g}}$  is the difference between dipole moment in the ground and excited state, and  $C$  is a constant. For a typical solvatochromic compound, the dependence of a Stokes shifts on  $\Delta f$  is linear in the absence of solvent-specific interactions, where the slope of the plot reflected solvatochromic sensitivity of a fluorophore. The most sensitive solvatochromic compounds are those with the steepest slope and therefore the largest change in the dipole moment. The Lippert–Magada plots of **PM3** showed the best

linear relationship and largest slopes, indicating that the dipole moment variation of **PM3** between ground-state and excited-state was largest among these **PM** compounds. The enhanced excited state dipole moment of the solute upon excitation induced the local dipole–dipole interactions that forced the reorientation of the polar solvent molecules around the excited solute.<sup>55</sup> This was accompanied by the molecular structural relaxation and gave rise to inhomogeneous broadening of the fluorescence spectrum with emission occurring from a relaxed state at lower energy.<sup>56</sup> Therefore, the emission spectra of **PM** compounds in ethanol and methanol were obviously broadened.

### Electrochemical properties

Knowledge of HOMO and LUMO energy levels of organic electronic materials, especially OLED materials, is important because they might affect the charge injection from adjacent layers. To further evaluate the potential applicability of the present **PM** compounds in electronic devices, cyclic voltammetry (CV) experiment was carried out to investigate their electrochemical properties. In this work, we measured the oxidation potentials of all **PM** compounds in DCM solution and used these electrochemical values to estimate the HOMO energy levels ( $E_{\text{HOMO}}$ ) versus ferrocene/ferrocenium ( $\text{Fc}/\text{Fc}^+$ ). The LUMO energy levels ( $E_{\text{LUMO}}$ ) were calculated from the  $E_{\text{HOMO}}$  and optical band gap. The oxidation potentials  $E_{\text{ox}}$ ,  $E_{\text{HOMO}}$  and  $E_{\text{LUMO}}$  values derived from CV were shown in Table 2.

One quasi-reversible oxidation peak was observed for each **PM** compound, as shown in Fig. S3.† For carbazole based **PM** compounds, **PM1** and **PM2**, the nature of the acceptor terminal had a small influence on the oxidation potentials. Compared to the carbazole-based compound CBP (4,4'-di(9H-carbazol-9-yl)biphenyl), which was a hole transporting (HT) emitter and widely utilized as HT host materials, the  $E_{\text{HOMO}}$  of **PM1** and **PM2** (−5.47 and −5.49 eV, respectively) were slightly higher than that of CBP (−5.50 eV).<sup>57</sup> Nevertheless, their  $E_{\text{LUMO}}$  (−2.16 and −2.20 eV) obtained from the HOMO and optical band gap were much lower than that of CBP (−2.0 eV).<sup>57</sup> The lower LUMO of **PM1** and **PM2** compared with that of CBP suggested that both of them had better electron injection and transfer abilities than CBP,

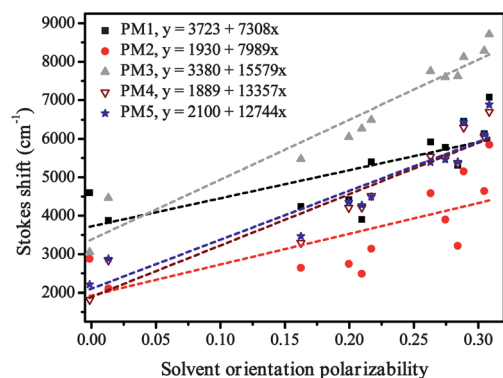


Fig. 3 Lippert–Magada plots of **PM1–PM5**. The  $y$  and  $x$  in the equations of the fitted lines represented Stokes shift and solvent orientation polarizability, respectively. The correlation coefficients ( $R^2$ ) of the fitted lines were 0.49, 0.45, 0.93, 0.89 and 0.87 in turn.

**Table 2** Experimental and theoretical HOMO, LUMO and singlet band gap of **PM1–PM5**

Molecule	From CV				B3LYP/6-31G(d)					
	$E_g^{\text{opta}}$ (eV)	$E_{\text{onset/peak}}^{\text{ox}}$ (V)	$E_{\text{HOMO}}$ (eV)	$E_{\text{LUMO}}^b$ (eV)	$E_g^{\text{calc}}$ (eV)	$E_{\text{HOMO}}^c$ (eV)	$E_{\text{LUMO}}^c$ (eV)	$E_g^{\text{cald}}$ (eV)	$E_{\text{HOMO}}^d$ (eV)	$E_{\text{LUMO}}^d$ (eV)
<b>PM1</b>	3.31	0.78/1.16	-5.47	-2.16	4.16	-5.48	-1.32	4.06	-5.54	-1.48
<b>PM2</b>	3.29	0.80/1.20	-5.49	-2.20	4.08	-5.63	-1.55	3.97	-5.64	-1.67
<b>PM3</b>	2.98	0.64/0.86	-5.33	-2.35	3.66	-5.15	-1.49	3.59	-5.21	-1.62
<b>PM4</b>	2.91	0.65/0.90	-5.34	-2.43	3.52	-5.31	-1.79	3.45	-5.30	-1.85
<b>PM5</b>	2.93	0.75/0.98	-5.44	-2.51	3.52	-5.44	-1.92	3.48	-5.37	-1.89

<sup>a</sup> Obtained from the optical gap (onset of absorption in DCM). <sup>b</sup>  $E_{\text{LUMO}} = E_{\text{HOMO}} + E_g^{\text{opt}}$ . <sup>c</sup> Theoretical values calculated by DFT at B3LYP/6-31G(d) in vacuum. <sup>d</sup> Theoretical values calculated by DFT at B3LYP/6-31G(d) in solvent (DCM) with polarizable continuum model (PCM).

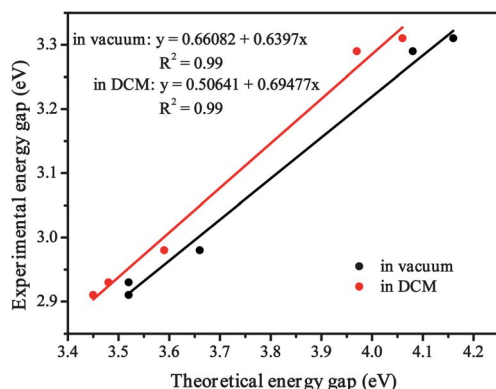
beneficial for charge injection balance. For the TPA based **PM** compounds, the  $E_{\text{HOMO}}$  of **PM3** and **PM4** were very close while the  $E_{\text{HOMO}}$  of **PM5** decreased by 0.1 eV compared to that of **PM4**. The more pyrimidin-4-yl substituents present resulted in larger decrease in  $E_{\text{HOMO}}$  in the following order: **PM3** > **PM4** > **PM5**, probably because of the electronegative nature of the pyrimidine moiety.

### Theoretical studies

To elucidate the influence of the structure on the electronic properties of **PM** compounds, theoretical calculations were performed using the Gaussian09 program package.<sup>58</sup> The optimizations of the molecular geometry and total energy calculations were carried out using density functional theory (DFT) calculations at B3LYP/6-31G(d) level.<sup>59</sup> All the optimized ground-state geometries are shown in the ESI (Tables S2–S6†).

As listed in Table 2, the HOMO and LUMO level energies and the energy gaps ( $E_g^{\text{cal}}$ ) both in vacuum and DCM were well predicted by DFT calculations with good correlation. Although the theoretical energy gaps of **PM1–PM5** were overestimated compared to the experimental values, excellent correlations could be found between the theoretical and experimental energy gaps (Fig. 4), which suggested that the DFT calculation results indeed provide good estimations of the energy gap trends.<sup>60</sup>

The frontier molecular orbital electron density distributions of the **PM** compounds are shown in Fig. 5. It can be seen that,

**Fig. 4** The relationship between the theoretical and experimental energy gap.

the HOMOs of all **PM** compounds are orbitals of  $\pi$  character delocalized over the entire molecules, suggesting that the HOMOs are determined by both carbazole/TPA and pyrimidine. The LUMOs of **PM1–PM4** are predominately localized on the terminal pyrimidine moieties and the aryl groups around them suggesting that the LUMOs are predominately determined by the pyrimidine. **PM5** is composed of three pyrimidin-4-yl-phenyl moieties with a central amine nitrogen atom. The central  $\text{NC}_3$  moiety is planar and forms an equilateral triangle. The pyrimidin-4-yl-phenyl moieties are symmetrically twisted from that plane so the whole molecule can be visualized as a propeller (Table 3). Although the optimized geometry of **PM5** is symmetrical, the LUMO diagram shows that the electron clouds are  $\pi$  orbitals delocalized mainly on two of the three pyrimidin-4-yl-phenyl moieties. It can be obviously seen that central nitrogen does not contribute to the LUMO of **PM5**, however, the pyrimidin-4-yl interacts with the phenyl ring.

The optoelectronic devices depend on the charge injection, transfer, as well as balance. It was necessary to investigate the ionization potentials (IPs), electronic affinity (EAs), and reorganization energies ( $\lambda$ ), so that we could evaluate the energy barrier for injection and transport rates of the holes and electrons. The IPs and EAs, together with the hole extraction potential (HEP) and electron extraction potential (EEP) for **PM1–PM5** were calculated by DFT and derived from the computed results according to literature publications.<sup>61–65</sup> The IP and EA values were used to evaluate the energy barrier for the injection of holes and electrons.<sup>61</sup> HEP is the energy difference between the neutral molecule (M) to cationic ( $\text{M}^+$ ) using the  $\text{M}^+$  geometric structure in the calculation, while EEP is the energy difference between the M to anionic ( $\text{M}^-$ ) using the  $\text{M}^-$  geometric structure.<sup>62,63,65</sup> In addition, the reorganization energy is the energy difference between the two molecules which have gone through electron transfer and provides a qualitative indication of the charge-transport rate (the lower the  $\lambda$  values, the bigger the charge-transport rate).<sup>65</sup>

As shown in Table 4, the IP values of **PM2** and **PM1** changed slightly (*ca.* 0.011 eV), while the EA values increased significantly (*ca.* 0.520 eV) from **PM1** to **PM2**. For the TPA based ones, both IP and EA values gradually increased in the following order: **PM3** < **PM4** < **PM5**, as more and more pyrimidin-4-yl moieties are introduced. The increase of EA values was much

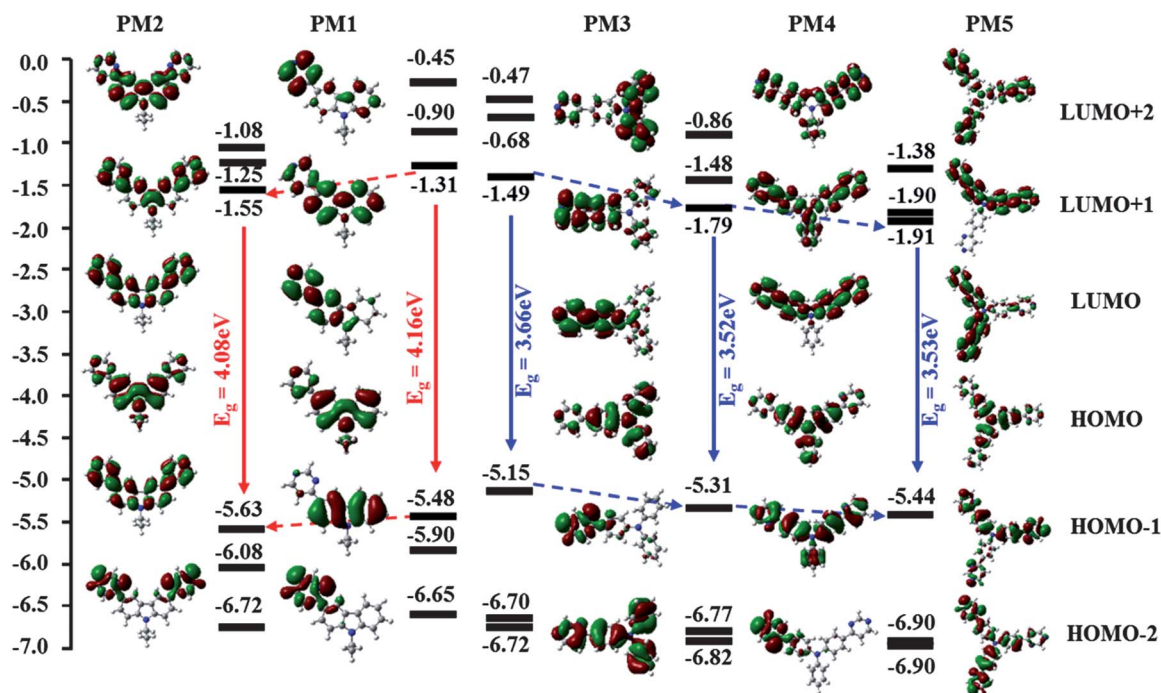


Fig. 5 The optimized ground geometries, frontier molecular orbital energies and electron density distributions of **PM1–PM5**.

larger than that of IP values, which demonstrates that the incorporation of pyrimidin-4-yl could benefit the electron-accepting ability. The negative calculated EA value of **PM1** was raised by the incomplete cancellation of electronic self-interaction energy due to the use of an inexact density functional and a finite basis set.<sup>66,67</sup>

The calculated reorganization energies are also listed in Table 4. The  $\lambda_{\text{hole}}$  values for **PM1–PM5** were all smaller than their respective  $\lambda_{\text{electron}}$  values, indicating that the hole transfer rate was higher than the electron transfer rate. As more and more pyrimidin-4-yl moieties are introduced, the  $\lambda_{\text{electron}}$  values decrease sharply with large variations while the  $\lambda_{\text{hole}}$  values hardly change. **PM2** and **PM5** have the smallest  $\lambda_{\text{electron}}$  for the **PM** compounds with a carbazole and a TPA unit, respectively, which suggested that **PM2** and **PM5** have a higher electron transfer rate. In addition, the difference between  $\lambda_{\text{hole}}$  and  $\lambda_{\text{electron}}$  gradually decreases in the following order: **PM1** (0.223 eV) < **PM2** (0.128 eV) and **PM3** (0.399 eV) < **PM4** (0.163 eV) < **PM5**

Table 4 Ionization potential (IP), electronic affinity (EA) and reorganization energy ( $\lambda$ ) of **PM1–PM5** by DFT at B3LYP/6-31G(d)<sup>a</sup> (in eV)

Molecule	IP (v)	IP (a)	HEP	EA (v)	EA (a)	EEP	$\lambda_{\text{hole}}$	$\lambda_{\text{electron}}$
<b>PM1</b>	6.935	6.880	6.822	-0.233	-0.070	0.104	0.113	0.336
<b>PM2</b>	6.946	6.890	6.837	0.287	0.412	0.525	0.110	0.238
<b>PM3</b>	6.483	6.424	6.368	0.036	0.301	0.550	0.114	0.513
<b>PM4</b>	6.540	6.483	6.429	0.608	0.747	0.882	0.110	0.273
<b>PM5</b>	6.586	6.532	6.480	0.822	0.925	1.025	0.105	0.203

<sup>a</sup> The IPs and EAs can be either for vertical excitations (v, at the geometry of the neutral molecule) or adiabatic excitations (a, optimized structure for both the neutral and charged molecule).

(0.098 eV), implying that **PM2** and **PM5** have better hole- and electron-transporting balance and could act as good ambipolar materials. Therefore, the pyrimidin-4-yl group was a nice electron-accepting candidate for designing ambipolar materials.

Table 3 The optimized ground geometry and relevant bond lengths, angles, and dihedrals of **PM5** by DFT at B3LYP/6-31G(d)

	Bond length (Å)	C1–N1	1.41898
		C2–N1	1.41896
		C3–N1	1.41941
Bond angle $\varphi$ (°)	C1–N1–C1'	119.96168	
	C2–N1–C2'	120.10335	
	C3–N1–C3'	119.93472	
Torsion angle $\theta$ (°)	C1'–C1–N1–C2	-40.46637	
	C2'–C2–N1–C3	-40.83949	
	C3'–C3–N1–C1	-40.03956	

In order to understand electronic transitions of **PM** compounds, time-dependent density functional theory (TD-DFT) calculations on the absorption spectra in both vacuum and solvent were performed. The calculated wavelengths from the absorption spectra, the main transition configurations, and the oscillator strengths for the most relevant singlet excited states of **PM** compounds were listed in Tables 5 and S7,<sup>†</sup> and the simulated absorption spectra are shown in Fig. S4.<sup>†</sup> All the electronic transitions of the **PM** compounds were of the  $\pi \rightarrow \pi^*$  type for the absorption spectra, where the electron transitions were from the initial state (predominately contributed by the HOMO) to the final state (predominately contributed by the LUMO). For carbazole based **PM** compounds, the maximum absorption wavelengths in vacuum exhibited a red-shift (*ca.* 12 nm) from **PM1** to **PM2**. The HOMO and LUMO energy levels of **PM1** are  $-5.48$  and  $-1.32$  eV, respectively. The calculated first excited state had an excitation energy of 3.76 eV (330.2 nm) with an oscillator strength of 0.2954. The incorporation of one more electron-drawing pyrimidin-4-yl at the 6-position of the carbazole ring (**PM2**) led to a decrease both in the HOMO and LUMO energy level by 0.15 and 0.23 eV, respectively. Consequently, the calculated first excited energy of **PM2** was reduced to 3.62 eV (342.5 nm). This change led to a notable increase in the oscillator strength of the first excited state ( $f = 0.4677$ ). For the TPA based **PM** compounds, the maximum absorption wavelengths in the vacuum gradually red-shifted in the following order: **PM3** (375.3 nm) < **PM4** (397.2 nm) < **PM5** (399.1 nm), which confirms the prediction from the energy gaps listed in Table 2. When three pyrimidin-4-yl groups were introduced onto 4,4',4''-positions of the TPA framework, both the HOMO and LUMO energy levels of **PM5** were lowered compared to those of **PM4**, but the calculated ground state energy gap was very close to that of **PM4**. The excitation energy of the first excited state of **PM5** was decreased slightly by 0.01 eV compared to **PM4**.

The influence of solvent (DCM) on the absorption spectra of the **PM** compounds was simulated by using the PCM model.<sup>61,64</sup> The maximum absorption wavelengths in DCM were larger than those in vacuum, indicating that the solvent effects stabilized the excited state, which induced the red-shift of the absorption spectra as compared with those in vacuum. The maximum absorption wavelengths in DCM gradually red-shifted in the

following order: **PM1** (344.5 nm) < **PM2** (357.3 nm) and **PM3** (393.7 nm) < **PM4** (415.2 nm), which are consistent with those in vacuum. However, it was interesting to note that the maximum absorption wavelength of **PM5** in DCM was slightly smaller (*ca.* 3 nm) than that of **PM4**, which was probably due to the decrease of the dipole moment of **PM5**. In both vacuum and in polar solvent DCM, the dipole moment of **PM4** was slightly shorter than that of **PM3**, and their  $\Delta\lambda_{\text{DCM-vacuum}}$  (the difference between the maximum absorption wavelength simulated in DCM and that in vacuum) was very close ( $\Delta\lambda_{\text{DCM-vacuum}} = 18.4$  nm and 18.0 nm for **PM3** and **PM4**, respectively). Compared to **PM3** and **PM4**, the dipole moment of **PM5** is much shorter, which is due to its symmetrical geometry. Therefore, the  $\Delta\lambda_{\text{DCM-vacuum}}$  of **PM5** (12.7 nm) is significant smaller than those of **PM3** and **PM4**. In conjunction with these changes, the absorption spectrum of **PM5** in DCM is slightly blue-shifted as compared with that of **PM4**. Whereas the accuracy of the calculated excitation energy is not high enough by the level of our calculations, these calculated results evidently demonstrate the nature of the transition significantly dependent on the electronic effect of the pyrimidin-4-yl substituent and the substitution number of the molecular structure. The introduction of the electron-drawing pyrimidin-4-yl groups onto electron donor (carbazole/TPA) led to efficient intramolecular CT transition for those D-A conjugated systems, which is consistent with our experimental results.

## Conclusions

A series of bipolar luminescent materials, **PM1–PM5**, containing 4-monosubstituted pyrimidine moieties as the electron acceptor, were synthesized using a  $\text{ZnCl}_2$ -catalyzed three-component coupling reaction and their optoelectronic properties were systematically studied. These **PM** compounds exhibited intense fluorescence in DCM at room temperature with fluorescence quantum yields of  $\sim 0.53$ – $0.93$ . Introducing more pyrimidin-4-yl moieties onto the carbazole or triphenylamine fragment, the maximum emission peaks in DCM solution blue shifted and hardly shifted in solid state. The CV data demonstrated that the HOMO level energies of these **PM** compounds slightly decreased when more pyrimidin-4-yl terminals were

**Table 5** The absorption spectra calculated by DFT at B3LYP/6-31G(d) in vacuum and solvent (DCM) of **PM1–PM5**

Molecule	States	Electron transition	Calculated wavelength (nm)	Excitation energy $E_{s1}$	Main transition configuration	Oscillator strength $f$	Dipole moment (Debye)
<b>PM1</b>	Gas-phase	$S_0-S_1$	330.2	3.76	HOMO $\rightarrow$ LUMO (0.92)	0.2954	5.1315
	DCM	$S_0-S_1$	344.5	3.60	HOMO $\rightarrow$ LUMO (0.96)	0.4228	6.5696
<b>PM2</b>	Gas-phase	$S_0-S_1$	342.5	3.62	HOMO $\rightarrow$ LUMO (0.96)	0.4677	7.7232
	DCM	$S_0-S_1$	357.3	3.47	HOMO $\rightarrow$ LUMO (0.98)	0.6355	10.1313
<b>PM3</b>	Gas-phase	$S_0-S_1$	375.3	3.30	HOMO $\rightarrow$ LUMO (0.99)	0.6056	3.9140
	DCM	$S_0-S_1$	393.7	3.15	HOMO $\rightarrow$ LUMO (0.99)	0.7083	4.8549
<b>PM4</b>	Gas-phase	$S_0-S_1$	397.2	3.12	HOMO $\rightarrow$ LUMO (0.99)	0.7848	3.7588
	DCM	$S_0-S_1$	415.2	2.99	HOMO $\rightarrow$ LUMO (0.99)	0.9041	4.7973
<b>PM5</b>	Gas-phase	$S_0-S_1$	399.1	3.11	HOMO $\rightarrow$ LUMO (0.99)	0.6520	3.0592
	DCM	$S_0-S_1$	411.8	3.01	HOMO $\rightarrow$ LUMO (0.99)	0.7685	4.2579

introduced. Both **PM1** and **PM2** had a lower LUMO than that of CBP, suggesting both of them had better electron injection and transfer abilities. Theoretical calculations were also performed to elucidate the influence of the structure on the electronic properties of **PM** compounds. The variation tendencies of energy levels and absorption spectra obtained from DFT calculation well agreed with the experiment data. The DFT study also suggested that the EAs and  $\lambda_{\text{electron}}$  of **PM** compounds could be modified effectively. The narrow differences between  $\lambda_{\text{hole}}$  and  $\lambda_{\text{electron}}$  were found in **PM2** and **PM5**, which implied that **PM2** and **PM5** could act as excellent ambipolar materials.

## Experimental section

### Materials

All reagents were purchased from commercial sources and were used without further purification, unless otherwise noted. In synthetic preparations, dichloromethane (DCM) were distilled from CaH<sub>2</sub>. Similarly, toluene was dried by distillation from sodium/benzophenone. 9-Ethyl-9H-carbazole (**ECz**) was prepared according to known literature procedures.<sup>68</sup>

### Characterization

The molecular structures of all newly synthesized compounds were unambiguously determined through NMR (<sup>1</sup>H and <sup>13</sup>C) and mass (GC-MS or MALDI-TOF-MS) spectroscopy. The NMR spectra were recorded with a Bruker Ultra Shield Plus 400 MHz spectrometer, with the chemical shifts reported in ppm using tetramethylsilane (TMS) as an internal standard. The concentrations of these compounds solution were adjusted to 10–12 mg mL<sup>-1</sup> and 20–30 mg mL<sup>-1</sup> for <sup>1</sup>H NMR and <sup>13</sup>C NMR experiments, respectively. Mass spectrometric data were obtained with a Shimadzu GCMS-QP 2010 Plus spectrometry or Bruker Daltonics matrix-assisted laser desorption/ionization time-of-flight mass spectrometer. UV-vis spectra were obtained using a Shimadzu UV-3600 UV-vis-NIR spectrophotometer using quartz cell. Room temperature fluorescence measurements were performed using Shimadzu RF-5301PC fluorescence spectrophotometer. For the spectra recorded in solution, the concentrations of all the materials were 1 × 10<sup>-5</sup> M. For the thin film spectra, materials (1 mg) were first dissolved in 1 mL of DCM containing PMMA (20 mg mL<sup>-1</sup>), and spin-coated at a speed rate of 1500 rpm for 30 s onto the quartz slides. The energy gaps ( $E_g$ ) were calculated from the edge of the visible-absorption bands in the DCM spectra ( $E_g = hc/\lambda_{\text{onset}}$ ). The cyclic voltammograms (CV) were performed using a CHI660C electrochemical workstation at room temperature. The measuring cell was composed of a glassy carbon as the working electrode, an Ag/AgNO<sub>3</sub> electrode as the reference electrode and a platinum wire as the auxiliary electrode. The electrodes were immersed in a DCM solution containing 0.1 M tetrabutylammonium perchlorate (*n*-Bu<sub>4</sub>NClO<sub>4</sub>) and 0.001 M **PM1–PM5**. The highest occupied molecular orbital (HOMO) energy levels of the materials were estimated based on the reference energy levels of ferrocene (Fc, -4.8 eV with respect to the vacuum level): HOMO =  $-[(E_{\text{ox}}^{\text{onset}} - 0.11) + 4.8]$  eV, where the value of 0.11 V

was for Fc vs. Ag/Ag<sup>+</sup> and  $E_{\text{ox}}^{\text{onset}}$  was the onset potential. The fluorescent quantum efficiency ( $\Phi$ ) was measured with 9,10-diphenylanthracene as a standard.<sup>69</sup>

### Quantum yield measurement

Fluorescence quantum yield was determined using optically matching solutions of 9,10-diphenylanthracene ( $\Phi_f = 0.9$  in cyclohexane) as standards at an excitation wavelength of 360 nm and the quantum yield was calculated using eqn (2).<sup>69</sup>

$$\Phi_{\text{unk}} = \Phi_{\text{std}} \left( \frac{I_{\text{unk}}/A_{\text{unk}}}{I_{\text{std}}/A_{\text{std}}} \right) \left( \frac{\eta_{\text{unk}}}{\eta_{\text{std}}} \right)^2 \quad (2)$$

where  $\Phi_{\text{unk}}$  and  $\Phi_{\text{std}}$  are the fluorescence quantum yields of the sample and the standard, respectively.  $I_{\text{unk}}$  and  $I_{\text{std}}$  are the integrated emission intensities of the sample and the standard, respectively.  $A_{\text{unk}}$  and  $A_{\text{std}}$  are the absorbance of the sample and the standard, respectively. And  $\eta_{\text{unk}}$  and  $\eta_{\text{std}}$  are the refractive indexes of the corresponding solutions.

### Synthesis

**General procedure of Friedel–Crafts acylation reaction.** The general synthesis protocols used to produce the acetyl-compounds were shown in Scheme 1. AlCl<sub>3</sub> (1.5 equiv. to 5 equiv.) and DCM were placed into a two neck-flask with a drying tube, acetyl chloride or acetic anhydride (1.2 equiv. to 3.6 equiv.) was added dropwise at 0 °C and stirred until AlCl<sub>3</sub> was completely dissolved. The mixture prepared above was removed to a dropping funnel and added dropwise to DCM solution containing **ECz** or **TPA** (1.0 equiv.) at 0 °C. The mixture was stirred at 0 °C for 1 h to 2 h. After warmed to room temperature slowly, the mixture was stirred at room temperature or at 40 °C and monitored by TLC analysis until the reaction had been completed. The mixture was poured into a large amount of ice water slowly and stirred until the inorganic layer was clear. The mixture was extracted several times with DCM, and the combined organic extracts were dried over Na<sub>2</sub>SO<sub>4</sub>, filtered, and then concentrated under reduced pressure. The crude product was purified by silica gel chromatography (ethyl acetate–petroleum ether) to produce acetyl-compound (**A1–A5**).

**General procedure for the synthesis of pyrimidine compounds.** To a toluene solution of ZnCl<sub>2</sub> (0.1 equiv. for an acetyl) and triethyl orthoformate (3 equiv. for an acetyl) was added acetyl-compound (1 equiv.) (**A1–A5**) and ammonium acetate (2 equiv. for an acetyl). The mixture was heated at 100 °C for 48 h. After cooled to room temperature, a saturated aqueous solution of NaHCO<sub>3</sub> was added to the mixture to quench the reaction. The mixture was extracted several times with DCM and the combined organic extracts were dried over Na<sub>2</sub>SO<sub>4</sub>, filtered, and then concentrated under reduced pressure. The crude product was purified by silica gel chromatography (ethyl acetate–petroleum ether) to produce pyrimidine compounds (**PM1–PM5**).

**1-(9-Ethyl-9H-carbazol-3-yl)-ethanone (A1).** 70% yield; a white solid; <sup>1</sup>H NMR (400 Hz, CDCl<sub>3</sub>)  $\delta$  (ppm): 8.75 (d,  $J = 1.4$  Hz, 1H), 8.20–8.10 (m, 2H), 7.53 (t,  $J = 7.5$  Hz, 1H), 7.43 (dd,  $J = 13.8, 8.4$  Hz, 2H), 7.31 (t,  $J = 7.4$  Hz, 1H), 4.40 (q,  $J = 7.2$  Hz, 2H), 2.73

(s, 3H), 1.46 (t,  $J = 7.2$  Hz, 3H);  $^{13}\text{C}$  NMR (100 MHz,  $\text{CDCl}_3$ )  $\delta$  (ppm): 197.70, 142.70, 140.66, 128.77, 126.47, 126.44, 123.28, 122.71, 121.94, 120.70, 119.99, 109.01, 108.04, 37.84, 26.67, 13.82. GC-MS: M, found 237.  $\text{C}_{16}\text{H}_{15}\text{NO}$  requires 237.30.

**1-(6-Acetyl-9-ethyl-9H-carbazol-3-yl)-ethanone (A2).** 63% yield; a white solid;  $^1\text{H}$  NMR (400 MHz,  $\text{CDCl}_3$ )  $\delta$  (ppm): 8.75–8.71 (m, 2H), 8.14 (dd,  $J = 8.6, 1.7$  Hz, 2H), 7.41 (dd,  $J = 8.6, 0.4$  Hz, 2H), 4.37 (q,  $J = 7.3$  Hz, 2H), 2.71 (s, 6H), 1.45 (t,  $J = 7.2$  Hz, 3H);  $^{13}\text{C}$  NMR (100 MHz,  $\text{CDCl}_3$ )  $\delta$  (ppm): 197.44, 143.35, 129.67, 127.00, 122.93, 121.97, 108.69, 38.14, 26.68, 13.85. GC-MS: M, found 279.  $\text{C}_{18}\text{H}_{17}\text{NO}_2$  requires 279.33.

**1-(4-Diphenylamino-phenyl)-ethanone (A3).** 75% yield; a white solid;  $^1\text{H}$  NMR (400 MHz,  $\text{CDCl}_3$ )  $\delta$  (ppm): 7.84–7.74 (m, 2H), 7.35–7.29 (m, 4H), 7.19–7.08 (m, 6H), 7.01–6.96 (m, 2H), 2.53 (s, 3H);  $^{13}\text{C}$  NMR (100 MHz,  $\text{CDCl}_3$ )  $\delta$  (ppm): 196.50, 152.19, 146.52, 129.90, 129.81, 129.62, 125.97, 124.64, 119.69, 26.24. GC-MS: M, found 287.  $\text{C}_{20}\text{H}_{17}\text{NO}$  requires 287.36.

**1-{4-[(4-Acetyl-phenyl)-phenyl-amino]-phenyl}-ethanone (A4).** 42% yield; a light yellow solid;  $^1\text{H}$  NMR (400 MHz,  $\text{CDCl}_3$ )  $\delta$  (ppm): 7.85 (d,  $J = 8.7$  Hz, 4H), 7.36 (t,  $J = 7.8$  Hz, 2H), 7.21 (t,  $J = 7.4$  Hz, 1H), 7.14 (d,  $J = 7.5$  Hz, 2H), 7.12 (dd,  $J = 17.4, 8.1$  Hz, 4H), 2.55 (s, 6H);  $^{13}\text{C}$  NMR (100 MHz,  $\text{CDCl}_3$ )  $\delta$  (ppm): 196.58, 151.05, 145.85, 131.67, 129.67, 126.73, 125.71, 122.40, 26.40. GC-MS: M, found 329.  $\text{C}_{20}\text{H}_{17}\text{NO}$  requires 329.39.

**1-{4-[Bis-(4-acetyl-phenyl)-amino]-phenyl}-ethanone (A5).** 70% yield; a yellow solid;  $^1\text{H}$  NMR (400 MHz,  $\text{CDCl}_3$ )  $\delta$  (ppm): 7.89 (d,  $J = 8.6$  Hz, 6H), 7.14 (d,  $J = 8.6$  Hz, 6H), 2.56 (s, 9H);  $^{13}\text{C}$  NMR (100 MHz,  $\text{CDCl}_3$ )  $\delta$  (ppm): 196.56, 150.31, 132.88, 130.14, 123.93, 26.48. GC-MS: M, found 371.  $\text{C}_{20}\text{H}_{17}\text{NO}$  requires 371.43.

**9-Ethyl-3-pyrimidin-4-yl-9H-carbazole (PM1).** 20% yield; a white solid;  $^1\text{H}$  NMR (400 MHz,  $\text{CDCl}_3$ )  $\delta$  (ppm): 9.27 (s, 1H), 8.90 (s, 1H), 8.72 (d,  $J = 5.4$  Hz, 1H), 8.20 (t,  $J = 8.4$  Hz, 2H), 7.80 (d,  $J = 5.5$  Hz, 1H), 7.48 (dq,  $J = 24.6, 8.1$  Hz, 3H), 7.30 (t,  $J = 7.4$  Hz, 1H), 4.39 (q,  $J = 7.2$  Hz, 2H), 1.46 (t,  $J = 7.2$  Hz, 3H);  $^{13}\text{C}$  NMR (100 MHz,  $\text{CDCl}_3$ )  $\delta$  (ppm): 164.57, 159.05, 157.07, 141.82, 140.59, 127.12, 126.35, 124.82, 123.57, 123.13, 120.76, 119.81, 119.70, 116.43, 108.90, 108.82, 37.80, 13.85. GC-MS: M, found 273.  $\text{C}_{18}\text{H}_{15}\text{N}_3$  requires 273.33.

**9-Ethyl-3, 6-di-pyrimidin-4-yl-9H-carbazole (PM2).** 14.5% yield; a white solid;  $^1\text{H}$  NMR (400 MHz,  $\text{CDCl}_3$ )  $\delta$  (ppm): 9.27 (s, 2H), 8.97 (s, 2H), 8.75 (d,  $J = 5.4$  Hz, 2H), 8.27 (dd,  $J = 8.6, 1.0$  Hz, 2H), 7.82 (d,  $J = 5.4$  Hz, 2H), 7.51 (d,  $J = 8.6$  Hz, 2H), 4.42 (q,  $J = 7.2$  Hz, 2H), 1.49 (t,  $J = 7.2$  Hz, 3H);  $^{13}\text{C}$  NMR (100 MHz,  $\text{CDCl}_3$ )  $\delta$  (ppm): 164.23, 159.09, 157.23, 142.42, 128.03, 125.45, 123.72, 120.05, 116.45, 109.30, 38.12, 13.92. GC-MS: M, found 351.  $\text{C}_{18}\text{H}_{15}\text{N}_3$  requires 351.40.

**Diphenyl-(4-pyrimidin-4-yl-phenyl)-amine (PM3).** 19% yield; a light yellow solid;  $^1\text{H}$  NMR (400 MHz,  $\text{CDCl}_3$ )  $\delta$  (ppm): 9.19 (s, 1H), 8.68 (d,  $J = 5.4$  Hz, 1H), 7.96 (d,  $J = 8.8$  Hz, 2H), 7.61 (dd,  $J = 5.5, 1.2$  Hz, 1H), 7.30 (t,  $J = 7.9$  Hz, 4H), 7.20–7.06 (m, 8H);  $^{13}\text{C}$  NMR (100 MHz,  $\text{CDCl}_3$ )  $\delta$  (ppm): 163.27, 159.04, 157.10, 150.71, 146.93, 129.52, 129.00, 128.10, 125.45, 124.07, 121.77, 116.01; GC-MS: M, found 323.  $\text{C}_{22}\text{H}_{17}\text{N}_3$  requires 323.39.

**Phenyl-bis-(4-pyrimidin-4-yl-phenyl)-amine (PM4).** 15% yield; a light yellow solid;  $^1\text{H}$  NMR (400 MHz,  $\text{CDCl}_3$ )  $\delta$  (ppm): 9.21 (d,  $J = 1.2$  Hz, 2H), 8.71 (d,  $J = 5.4$  Hz, 2H), 8.05–7.95 (m, 4H), 7.65 (dd,  $J = 5.4, 1.3$  Hz, 2H), 7.38–7.31 (m, 2H), 7.24–7.15

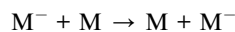
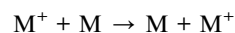
(m, 7H);  $^{13}\text{C}$  NMR (100 MHz,  $\text{CDCl}_3$ )  $\delta$  (ppm): 163.08, 159.09, 157.28, 149.82, 146.35, 130.59, 129.78, 128.30, 126.13, 124.98, 123.50, 116.25; MALDI-TOF-MS: M, found 401.359.  $\text{C}_{22}\text{H}_{17}\text{N}_3$  requires 401.463.

**Tris-(4-pyrimidin-4-yl-phenyl)-amine (PM5).** 12% yield; a yellow solid;  $^1\text{H}$  NMR (400 MHz,  $\text{CDCl}_3$ )  $\delta$  (ppm): 9.23 (d,  $J = 1.2$  Hz, 3H), 8.74 (d,  $J = 5.4$  Hz, 3H), 8.08–8.03 (m, 6H), 7.67 (dd,  $J = 5.4, 1.3$  Hz, 3H), 7.32–7.26 (m, 6H);  $^{13}\text{C}$  NMR (100 MHz,  $\text{CDCl}_3$ )  $\delta$  (ppm): 162.93, 159.13, 157.42, 149.18, 131.73, 128.52, 124.59, 116.42; MALDI-TOF-MS: M, found 479.531.  $\text{C}_{22}\text{H}_{17}\text{N}_3$  requires 479.535.

### Theoretical and computational methodology

All computations were done with Gaussian09 program package with different parameters for structure optimizations and vibrational analysis. The singlet ground-state geometries were fully optimized by the Becke's three-parameter exchange functional<sup>59</sup> along with the Lee–Yang–Parr correlation functional with the restricted (B3LYP) and the unrestricted formalism (UB3LYP) for neutral and ion state molecules<sup>70</sup> at the standard split valence plus polarization function 6-31G(d) basis set. The fully optimized stationary points were further characterized by harmonic vibrational frequency analysis to ensure that real local minima had been found without imaginary vibrational frequency. The electronic absorption spectra in vacuum were performed using TD-DFT method of B3LYP/6-31G(d) on the basis of the optimized ground structures. The polarizable continuum model (PCM) was adopted in TD-DFT calculation of the absorption spectra in the solvent (DCM).

Generally, organic  $\pi$ -conjugated materials were assumed to transport charge at room temperature *via* a thermally activated hopping-type mechanism.<sup>71–73</sup> The charge transport was the intermolecular process in which the charge hopped between two molecules, which can be summarized as follows:



where M represented the neutral molecule interacting with neighboring oxidized or reduced  $\text{M}^{+/-}$ . The standard Marcus–Hush equation<sup>74,75</sup> approximately described the hole/electron transfer rate, assuming that hole/electron traps were degenerate:

$$K_{\text{hole/electron}} = \left( \frac{\pi}{\lambda_{\text{hole/electron}} k T} \right)^{1/2} \frac{V_{\text{hole/electron}}^2}{\hbar} \exp \left( - \frac{\lambda_{\text{hole/electron}}}{4k T} \right)$$

where  $T$  is the temperature,  $V_{\text{hole/electron}}$  is the electronic coupling matrix element between neighboring molecules in the organic singlet crystal,  $k$  and  $\hbar$  refer to the Boltzmann constant and Planck constants, respectively.  $\lambda_{\text{hole/electron}}$  is the hole/electron reorganization energy due to geometric relaxation accompanying charge transfer, which was calculated by using the adiabatic potential energy surfaces method.<sup>64</sup> Experimentally,  $V_{\text{hole/electron}}$  showed a rather narrow range of values,<sup>71</sup> and an even more limited range of was expected due to the direct contacts in amorphous solids. Therefore, the hole/electron

mobility of PM compounds in our work was considered to be dominated by  $\lambda_{\text{hole/electron}}$  without  $V_{\text{hole/electron}}$ .

## Acknowledgements

This work was financially supported by the National Basic Research Program of China (973 Program, 2009CB930601), the National Natural Science Foundation of China (Project no. 50803027, no. 50903001, no. 20905038), and the Program for Postgraduates Research Innovation of Colleges and Universities in Jiangsu Province (CXLX11\_0421), the Research Fund for Nanjing University of Posts and Telecommunications (NY212074), the Natural Science Foundation from Bureau of Education of Anhui Province (KJ2013A108).

## Notes and references

- C. W. Tang and S. A. VanSlyke, *Appl. Phys. Lett.*, 1987, **51**, 913–915.
- B. X. Mi, Z. Q. Gao, Z. J. Liao, W. Huang and C. H. Chen, *Sci. China: Chem.*, 2010, **53**, 1679–1694.
- Y. Shirota and H. Kageyama, *Chem. Rev.*, 2007, **107**, 953–1010.
- Y. Shirota, *J. Mater. Chem.*, 2005, **15**, 75–93.
- Y. Shirota, *J. Mater. Chem.*, 2000, **10**, 1–25.
- L. Xiao, Z. Chen, B. Qu, S. Kong, Q. Gong and J. Kido, *Adv. Mater.*, 2011, **23**, 926–952.
- S. C. Lo and P. L. Burn, *Chem. Rev.*, 2007, **107**, 1097–1116.
- S. Zhang, R. Chen, J. Yin, F. Liu, H. Jiang, N. Shi, Z. An, C. Ma, B. Liu and W. Huang, *Org. Lett.*, 2010, **12**, 3438–3441.
- F. M. Hsu, C. H. Chien, P. I. Shih and C. F. Shu, *Chem. Mater.*, 2009, **21**, 1017–1022.
- J. He, H. M. Liu, Y. F. Dai, X. M. Qu, J. Wang, S. Tao, X. H. Zhang, P. F. Wang and D. G. Ma, *J. Phys. Chem. C*, 2009, **113**, 6761–6767.
- Y. T. Tao, Q. Wang, C. L. Yang, C. Zhong, K. Zhang, J. G. Qin and D. G. Ma, *Adv. Funct. Mater.*, 2010, **20**, 304–311.
- R. M. Adhikari, R. Mondal, B. K. Shah and D. C. Neckers, *J. Org. Chem.*, 2007, **72**, 4727–4732.
- X. Jiang, R. A. Register, A. Richard, K. A. Killeen, M. E. Thompson, F. Pschenitzka and J. C. Sturm, *Chem. Mater.*, 2000, **12**, 2542–2549.
- S. J. Su, C. Cai and J. Kido, *Chem. Mater.*, 2011, **23**, 274–284.
- A. Chasker, H. F. Chen and K. T. Wong, *Adv. Mater.*, 2011, **23**, 3876–3895.
- P. I. Shih, C. H. Chien, F. I. Wu and C. F. Shu, *Adv. Funct. Mater.*, 2007, **17**, 3514–3520.
- M. F. Wu, S. J. Yeh, C. T. Chen, H. Murayama, T. Tsuboi, W. S. Li, I. Chao, S. H. Liu and J. K. Wang, *Adv. Funct. Mater.*, 2007, **17**, 1887–1895.
- T. Tsuzuki and S. Tokito, *Appl. Phys. Lett.*, 2009, **94**, 33302.
- L. D. Hou, L. Duan, J. Qiao, W. Li, D. Q. Zhang and Y. Qiu, *Appl. Phys. Lett.*, 2008, **92**, 263301.
- H. H. Chou and C. H. Cheng, *Adv. Mater.*, 2010, **22**, 2468–2471.
- S. O. Jeon, K. S. Yook, C. W. Joo and J. Y. Lee, *Adv. Mater.*, 2010, **22**, 1872–1876.
- Y. Tao, Q. Wang, C. Yang, Z. Zhang, T. Zou, J. Qin and D. Ma, *Angew. Chem., Int. Ed.*, 2008, **47**, 8104–8107.
- X. Cai, A. B. Padmaperuma, L. S. Sapochak, P. A. Vecchi and P. E. Burrows, *Appl. Phys. Lett.*, 2008, **92**, 83308.
- S. O. Jeon, K. S. Yook, C. W. Joo, J. Y. Lee, K. Y. Ko, J. Y. Park and Y. G. Baek, *Appl. Phys. Lett.*, 2008, **93**, 63306.
- C. H. Chen, W. S. Huang, M. Y. Lai, W. C. Tsao, J. T. Lin, Y. H. Wu, T. H. Ke, L. Y. Chen and C. C. Wu, *Adv. Funct. Mater.*, 2009, **19**, 2661–2670.
- Z. Ge, T. Hayakawa, S. Ando, M. Ueda, T. Akiike, H. Miyamoto, T. Kajita and M. Kakimoto, *Chem. Mater.*, 2008, **20**, 2532–2537.
- S. Y. Takizawa, V. A. Montes and P. Anzenbacher, Jr, *Chem. Mater.*, 2009, **21**, 2452–2458.
- Z. Ge, T. Hayakawa, S. Ando, M. Ueda, T. Akiike, H. Miyamoto, T. Kajita and M. Kakimoto, *Adv. Funct. Mater.*, 2008, **18**, 584–590.
- K. E. Linton, A. L. Fisher, C. Pearson, M. A. Fox, L. O. Palsson, M. R. Bryce and M. C. Petty, *J. Mater. Chem.*, 2012, **22**, 11816–11825.
- M. K. Leung, C. C. Yang, J. H. Lee, H. H. Tsai, C. F. Lin, C. Y. Huang, O. Y. Su and C. F. Chiu, *Org. Lett.*, 2007, **9**, 235–238.
- H. F. Chen, S. J. Yang, Z. H. Tsai, W. Y. Hung, T. C. Wang and K. T. Wong, *J. Mater. Chem.*, 2009, **19**, 8112–8118.
- H. Inomata, K. Goushi, T. Masuko, T. Konno, T. Imai, H. Sasabe, J. J. Brown and C. Adachi, *Chem. Mater.*, 2004, **16**, 1285–1291.
- M. M. Rothmann, S. Haneder, E. Da Como, C. Lennartz, C. Schildknecht and P. Stroehriegel, *Chem. Mater.*, 2010, **22**, 2403–2410.
- S. J. Su, H. Sasabe, T. Takeda and J. Kido, *Chem. Mater.*, 2008, **20**, 1691–1693.
- A. B. Padmaperuma, L. S. Sapochak and P. E. Burrows, *Chem. Mater.*, 2006, **18**, 2389–2396.
- P. A. Vecchi, A. B. Padmaperuma, H. Qiao, L. S. Sapochak and P. E. Burrows, *Org. Lett.*, 2006, **8**, 4211–4214.
- S. O. Jeon and Y. J. Lee, *J. Mater. Chem.*, 2012, **22**, 4233–4243.
- V. V. Jarikov and D. Y. Kondakov, *J. Appl. Phys.*, 2009, **105**, 34905.
- D. Y. Kondakov, C. T. Brown, T. D. Pawlik and V. V. Jarikov, *J. Appl. Phys.*, 2010, **107**, 24507.
- R. Gompper, H. Mair and K. Polborn, *Synthesis*, 1997, 696–718.
- T. Kanbara, T. Kushida, N. Saito, I. Kuwajima, K. Kubota and T. Yamamoto, *Chem. Lett.*, 1992, **21**, 583–586.
- C. C. Wu, Y. T. Lin, H. H. Chiang, T. Y. Cho and C. W. Chen, *Appl. Phys. Lett.*, 2002, **81**, 577–579.
- M. Liu, S. J. Su, M. C. Jung, Y. Qi, W. M. Zhao and J. Kido, *Chem. Mater.*, 2012, **24**, 3817–3827.
- J. W. Goodby, M. Hird, R. A. Lewis and K. J. Toyne, *Chem. Commun.*, 1996, 2179–2180.
- S. J. Su, C. Cai and J. Kido, *J. Mater. Chem.*, 2012, **22**, 3447–3456.
- H. Sasabe, D. Tanaka, D. Yokoyama, T. Chiba, Y. Pu, K. Nakayama, M. Yokoyama and J. Kido, *Adv. Funct. Mater.*, 2011, **21**, 336–342.

- 47 R. Carlson, T. Lejon, T. Lundstedt and E. Le Clouerec, *Acta Chem. Scand.*, 1993, **47**, 1046–1049.
- 48 T. Ingebrigtsen, I. Helland and T. Lejon, *Heterocycles*, 2005, **65**, 2593–2603.
- 49 S. Tyagarajan and P. K. Chakravarty, *Tetrahedron Lett.*, 2005, **46**, 7889–7891.
- 50 I. Helland and T. Lejon, *Heterocycles*, 1999, **51**, 611–615.
- 51 T. Sasada, F. Kobayashi, N. Sakai and T. Konakahara, *Org. Lett.*, 2009, **11**, 2161–2164.
- 52 T. Yamamoto, Z. H. Zhou, T. Kanbara, M. Shimura, K. Kizu, T. Maruyama, Y. Nakamura, T. Fukuda, B. L. Lee, N. Ooba, S. Tomaru, T. Kurihara, T. Kaino, K. Kubota and S. Sasaki, *J. Am. Chem. Soc.*, 1996, **118**, 10389–10399.
- 53 Q. T. Zhang and J. M. Tours, *J. Am. Chem. Soc.*, 1998, **120**, 5355–5362.
- 54 J. R. Lakowich, *Principles of Fluorescence Spectroscopy*, Springer, New York, 2006.
- 55 Y. H. Zheng, A. S. Batsanov, V. Jankus, F. B. Dias, R. B. Matrin and A. P. Monkman, *J. Org. Chem.*, 2011, **76**, 8300–8310.
- 56 F. B. Dias, S. Pollock, G. Hedley, L. O. Pålsson, A. P. Monkman, I. I. Perepichka, I. F. Perepichka, M. Tavasli and M. R. Bryce, *J. Phys. Chem. B*, 2006, **110**, 19329–19339.
- 57 C. H. Chen, I. F. Wu, C. F. Shu, C. H. Chien and Y. T. Tao, *J. Mater. Chem.*, 2004, **14**, 1585–1589.
- 58 M. J. Frisch, G. W. Trucks, H. B. Schlegel, G. E. Scuseria, M. A. Robb, J. R. Cheeseman, G. Scalmani, V. Barone, B. Mennucci, G. A. Petersson, H. Nakatsuji, M. Caricato, X. Li, H. P. Hratchian, A. F. Izmaylov, J. Bloino, G. Zheng, J. L. Sonnenberg, M. Hada, M. Ehara, K. Toyota, R. Fukuda, J. Hasegawa, M. Ishida, T. Nakajima, Y. Honda, O. Kitao, H. Nakai, T. Vreven, J. A. Montgomery, Jr, J. E. Peralta, F. Ogliaro, M. Bearpark, J. J. Heyd, E. Brothers, K. N. Kudin, V. N. Staroverov, R. Kobayashi, J. Normand, K. Raghavachari, A. Rendell, J. C. Burant, S. S. Iyengar, J. Tomasi, M. Cossi, N. Rega, J. M. Millam, M. Klene, J. E. Knox, J. B. Cross, V. Bakken, C. Adamo, J. Jaramillo, R. Gomperts, R. E. Stratmann, O. Yazyev, A. J. Austin, R. Cammi, C. Pomelli, J. W. Ochterski, R. L. Martin, K. Morokuma, V. G. Zakrzewski, G. A. Voth, P. Salvador, J. J. Dannenberg, S. Dapprich, A. D. Daniels, O. Farkas, J. B. Foresman, J. V. Ortiz, J. Cioslowski and D. J. Fox, *Gaussian 09, Revision A.01*, Gaussian, Inc., Wallingford CT, 2009.
- 59 A. D. Becke, *J. Chem. Phys.*, 1993, **98**, 5648–5652.
- 60 N. Blouin, A. Michaud, D. Gendron, S. Wakim, E. Blair, R. Neagu-Plesu, M. Belletete, G. Durocher, Y. Tao and M. Leclerc, *J. Am. Chem. Soc.*, 2008, **130**, 732–742.
- 61 Y. Liu, J. Feng and A. Ren, *J. Comput. Chem.*, 2007, **28**, 2500–2509.
- 62 L. Y. Zou, A. M. Ren, J. K. Feng, Y. L. Liu, X. Q. Ran and C. C. Sun, *J. Phys. Chem. A*, 2008, **112**, 12172–12178.
- 63 J. Yin, R. Chen, S. Zhang, Q. Ling and W. Huang, *J. Phys. Chem. A*, 2010, **114**, 3655–3667.
- 64 X. Q. Ran, J. K. Feng, A. M. Ren, W. C. Li, L. Y. Zou and C. C. Sun, *J. Phys. Chem. A*, 2009, **113**, 7933–7939.
- 65 J. Yin, S. L. Zhang, R. F. Chen, Q. D. Ling and W. Huang, *Phys. Chem. Chem. Phys.*, 2010, **12**, 15448–15458.
- 66 J. C. Rienstra-Kiracofe, G. S. Tschumper, H. F. Schaefer, S. Nandi and G. B. Ellison, *Chem. Rev.*, 2002, **102**, 231–282.
- 67 X. F. Li, Z. L. Cai and M. D. Sevilla, *J. Phys. Chem. A*, 2002, **106**, 1596–1603.
- 68 G. Saikia and P. K. Iyer, *J. Org. Chem.*, 2010, **75**, 2714–2717.
- 69 S. Hamai and F. Hirayama, *J. Phys. Chem.*, 1983, **87**, 83–89.
- 70 C. Lee, W. Yang and R. G. Parr, *Phys. Rev. B*, 1988, **37**, 785–789.
- 71 S. F. Nelsen, D. A. Trieber, R. F. Ismagilov and Y. Teki, *J. Am. Chem. Soc.*, 2001, **123**, 5684–5694.
- 72 B. C. Lin, C. P. Cheng, Z. Q. You and C. P. Hsu, *J. Am. Chem. Soc.*, 2005, **127**, 66–67.
- 73 G. R. Hulchison, M. A. Ratner and T. J. Marks, *J. Am. Chem. Soc.*, 2005, **127**, 2339–2350.
- 74 R. A. Marcus and H. Eyring, *Annu. Rev. Phys. Chem.*, 1964, **15**, 155–196.
- 75 R. A. Marcus, *Rev. Mod. Phys.*, 1993, **65**, 599–610.